Dimerization of the C-type lectin-like receptor CD93 promotes its binding to Multimerin-2 in endothelial cells

Stefano Barbera [a,b], Luisa Raucci [a], Giusy Tassone [a], Laura Tinti [c], Filippo Prischi [d], Annalisa Santucci [a], Maurizio Mongiat [e], Gian Marco Tosi [f], Federico Galvagni [a], Anna Dimberg [b], Cecilia Pozzi [a,*], Maurizio Orlandini [a,**]

[a] Department of Biotechnology, Chemistry and Pharmacy, University of Siena, Siena 53100, Italy
[b] Department of Immunology, Genetics and Pathology, Science for Life Laboratory, Uppsala University, Rudbeck Laboratory, Uppsala SE-75185, Sweden
[c] Toscana Life Sciences Foundation, Siena 53100, Italy
[d] School of Life Sciences, University of Essex, Colchester CO4 3SQ, United Kingdom
[e] Department of Research and Diagnosis, Division of Molecular Oncology, Centro di Riferimento Oncologico di Aviano (CRO) IRCCS, Aviano 33081, Italy
[f] Department of Medicine, Surgery and Neuroscience, Ophthalmology Unit, University of Siena, Siena, 53100, Italy

ARTICLE INFO

ABSTRACT

Blocking the signaling activated by the plasma membrane receptor CD93 has recently been demonstrated a useful tool in antiangiogenic treatment and oncotherapy. In the proliferating endothelium, CD93 regulates cell adhesion, migration, and vascular maturation, yet it is unclear how CD93 interacts with the extracellular matrix activating signaling pathways involved in the vascular remodeling. Here for the first time we show that in endothelial cells CD93 is structured as a dimer and that this oligomeric form is physiologically instrumental for the binding of CD93 to its ligand Multimerin-2. Crystallographic X-ray analysis of recombinant CD93 reveals the crucial role played by the C-type lectin-like and sushi-like domains in arranging as an antiparallel dimer to achieve a functional binding state, providing key information for the future design of new drugs able to hamper CD93 function in neovascular pathologies.

1. Introduction

Blood vessel formation is required for development, growth, and wound healing, but when deregulated it contributes to numerous disorders [1]. Therefore, targeting blood vessels with antiangiogenic drugs has always been an appealing concept and the discovery of new molecular markers exploitable for the development of innovative strategies has become crucial to overcome the issues of the current antiangiogenic therapies [2].

CD93 is a single-pass transmembrane protein and member of the group 14 of the C-type lectin-like domain (CTLD) superfamily, which also includes endosialin/CD248, thrombomodulin, and CLEC14A [3]. CD93, from the N- to the C-terminus, consists of a conserved CTLD (designated as D1), a sushi-like domain (DX), five EGF-like repeats (D2), a heavily glycosylated mucin-like region (D3), a transmembrane domain (D4), and a short cytotail (D5) [4]. An increasing number of evidence suggests a key role played by CD93 in controlling the function of endothelial cells (ECs) and affecting angiogenesis [5]. CD93-deficient primary ECs, as well as ECs challenged with CD93 blocking antibodies, show aberrant actin cytoskeleton organization and reduced adhesion, migration, proliferation, and tube formation [6,7]. Impaired EC cytoskeletal organization was observed in time-lapse live imaging experiments showing that CD93-silenced ECs display high density of stress fibers, a phenotype associated with reduced migration velocity and poor organization of pro-migratory lamellipodia [8]. Importantly, knockout of CD93 in zebrafish embryos causes defects in the vascular system development [9], while in the mouse retina model the abrogation of CD93 reduces the number of endothelial tip cell filopodia [10]. Membrane receptors act by converting the signals deriving from extracellular cues into specific cellular responses. Consistently, Src-dependent phosphorylation of the CD93 cytoplasmic domain, triggered by interaction with the extracellular matrix (ECM), is required for the binding of the adaptor protein Cbl thus promoting EC migration and tube formation [11]. Indeed, in adhering and migrating ECs, CD93

promotes Cbl phosphorylation whereas in lamellipodia the CD93/phospho-Cbl association triggers a signaling axis, which in turn modulates the activity of small GTPases [8,12]. The receptor nature of CD93 is supported by the discovery that CD93 binds the ECM pan-endothelial glycoprotein Multimerin-2 [4,13,14] and, as recently reported, also the insulin-like growth factor binding protein 7 (IGFBP7), although via a different extracellular domain from that involved in the interaction with Multimerin-2 [15]. The binding of CD93 to Multimerin-2 promotes EC migration and tube formation and triggers the activation of β1 integrin through a CD93/Multimerin-2/active β1 integrin complex, thus promoting fibronectin deposition and remodeling [10]. Interestingly, these complexes are internalized via Rab5C-positive endosomes and recycled back to the plasma membrane during EC spreading and migration [16]. Noteworthy, plasma membrane levels of CD93 are also regulated by its intracellular domain, which harbors a binding site for Moesin required to connect CD93 to the actin cytoskeleton [17]. Indeed, a CD93 mutant lacking the cytoplasmic domain failed to efficiently reach the plasma membrane during EC migration [16].

CD93 has been demonstrated to be an attractive target for the treatment of cancer, as well as diseases associated with the overgrowth of blood vessels [18–20]. Intriguingly, the CD93 targeting has been shown to be potentially beneficial for the treatment of cancer and a novel promising approach for oncotherapy [15]. However, to achieve this goal and fulfill the promises of an effective anti-CD93 therapy, further knowledge is needed to dissect the role and function of the CD93 receptor. Here we demonstrate that in ECs CD93 is physiologically structured as a dimer and describe for the first time the structure of the CTLD-sushi region of CD93 at a resolution of 1.92 Å. The crystal structure reveals a surprising CD93 dimeric arrangement, elucidating its involvement in the cell-cell and cell-ECM adhesion phenomena.

2. Results

2.1. CD93 forms dimers on the EC surface

We have previously identified CD93 as a key receptor of a signaling pathway that selectively promotes cytoskeletal remodeling and cell migration in ECs [8,12]. While we were analyzing lysates from migrating human umbilical vein ECs (HUVECs) by immunoblotting, we observed that under non-reducing conditions the antibody 4E1, which recognizes a conformational epitope on the extracellular domain of CD93 [7], revealed the presence of a band with double the molecular
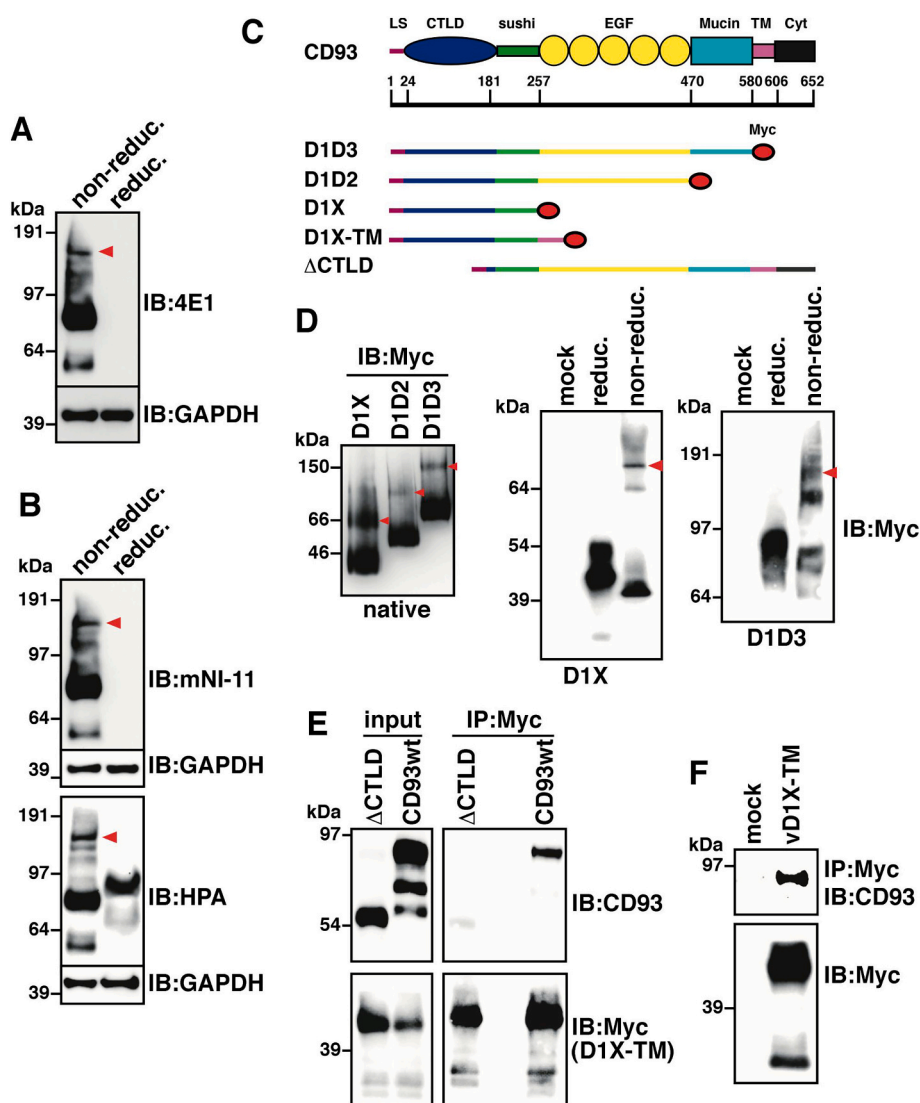

Fig. 1. CD93 is structured as a dimer. A and B: Cell extracts from migrating HUVECs were separated by SDS-PAGE under reducing (reduc.) or non-reducing (non-reduc.) conditions and subjected to immunoblotting analysis using the anti-CD93 antibodies 4E1, mNI-11, and HPA, as indicated. Red arrowheads indicate the position of the CD93 dimers. To confirm equal loading, whole cell extracts were analyzed by Western blotting with anti-GAPDH antibodies. C: Schematic representation of the deletion mutants generated for human CD93. A drawing of the CD93 full-length sequence is reported on the top. The numbers referring to the position of the amino acid residues of the mutants are reported. LS, leader sequence; CTLD, C-type lectin-like domain; sushi, sushi domain; EGF, EGF-like repeats; Mucin, mucin-like domain; TM, transmembrane domain; Cyt, cytoplasmic domain; Myc, 6 x Myc tag. D: Immunoblotting analysis of the cell supernatants from HEK 293 cells transfected with soluble Myc-tagged deletion mutants of CD93, using an anti-Myc antibody. Cell supernatants were subjected to electrophoresis under native, reducing (reduc.) or non-reducing (non-reduc.) conditions. Supernatants from cells transfected with an empty vector (mock) were analyzed under non-reducing conditions. The D1X, D1D2, and D1D3 mutants, covering respectively the amino acid residues from 1 to 257, from 1 to 470, and from 1 to 580 of the human CD93 sequence, are indicated. Red arrowheads indicate the position of the CD93 dimers. E: Cell extracts from HEK 293 cells transfected with the Myc-tagged membrane bound D1X mutant (D1X-TM) together with wild type CD93 or a CD93 mutant lacking the CTLD domain (ΔCTLD) were immunoprecipitated (IP) with anti-Myc antibodies. Immunoprecipitates were analyzed by immunoblotting (IB) with antibodies against CD93 and Myc to confirm equal loading. To check the expression of the mutant in HEK 293 cells, whole cell lysates were analyzed by Western blotting using antibodies against CD93 and Myc (input). F: Cell extracts from HUVECs transduced with an empty vector (mock) or a lentiviral construct expressing the Myc-tagged D1X-TM mutant (vD1X-TM) were immunoprecipitated (IP) using anti-Myc antibodies. Immunoprecipitates were analyzed by immunoblotting (IB) using antibodies against CD93 and Myc to confirm mutant expression.

weight of CD93 (Fig. 1A). Since some CTLD-containing proteins are involved in dimer formation [3], we further investigated the formation and role of the putative CD93 dimer. First, to rule out the possibility that the high molecular weight band was due to antibody cross-reactions, we analyzed the same HUVEC lysates by immunoblotting using two different monoclonal antibodies that recognize respectively a conformational and linear epitope on the extracellular domain of CD93. Under non-reducing conditions, both antibodies highlighted the high molecular weight band of CD93, further supporting the presence of a dimeric form (Fig. 1B). Next, to assess whether besides the transmembrane protein also the soluble forms of CD93 could dimerize, we expressed the previously described soluble Myc-tagged CD93 deletion mutants (Fig. 1C) [4] in HEK 293 cells and performed immunoblotting analyses of the cell culture supernatants. Under native and non-reducing conditions, the soluble extracellular CD93 fragments dimerized (Fig. 1D), also indicating the central role played by the CTLD-sushi region (namely D1X) in dimer formation. To corroborate the involvement of D1X in the dimerization of CD93, we co-transfected HEK 293 cells, which do not express endogenous CD93 [7], with a construct expressing the Myc-tagged membrane bound D1X mutant (D1X-TM) together with the wild type CD93 or a CD93 mutant lacking the CTLD domain (named ΔCTLD) (Fig. 1C). Importantly, although both the deletion mutants were properly expressed on the cell surface (Fig. S1), in co-immunoprecipitation experiments D1X-TM bound to the full-length CD93 but failed to bind to the mutant lacking the CTLD domain (Fig. 1E). Furthermore, in HUVECs transduced with a lentiviral construct expressing D1X-TM (vD1X-TM), the deletion mutant co-immunoprecipitated endogenous CD93 (Fig. 1F). Altogether, the above results led us to postulate that the CTLD domain could play a key role in CD93 dimerization. To verify this hypothesis, we sought to finely characterize CD93 protein-protein associations in ECs by fluorescence resonance energy transfer (FRET) analysis [21]. HUVECs were therefore transiently transfected with CD93-YFP together with CD93-CFP or ΔCTLD-CFP. In migrating ECs transfected with both plasmids expressing wild type CD93, photobleaching of the acceptor fluorophore (CD93-YFP) significantly increased the fluorescence intensity of the donor (CD93-CFP), whereas co-expression of CD93-YFP and ΔCTLD-CFP did

not (Fig. 2), suggesting that the CTLD domain is instrumental for structuring CD93 as a dimer. Interestingly, further analyses of more discrete cell regions within the photobleached area showed that FRET efficiency of wild type CD93 was significantly increased at the cell edge in comparison to the cytoplasmic signal (Fig. 2B).

2.2. The CD93 dimer binds to Multimerin-2

The results above indicate that during EC migration, CD93 is prone to dimerize via its CTLD domain. Since the CD93/Multimerin-2 interaction is crucial for proper EC migration [4], we asked whether the dimeric form of CD93 could bind to Multimerin-2. To address this question, we first expressed on large scale the extracellular region of CD93 (D1D3-His construct) in HEK 293 cells and, after nickel-affinity purification, the soluble protein was separated by size exclusion chromatography (Fig. S2). Western blot analysis confirmed the monomer separation from the dimer (Fig. 3A). The two protein forms were next tested for their ability to interact with Multimerin-2 and EMILIN2, an ECM protein that belongs to the EDEN protein family but is unable to bind to CD93 [4,22]. Intriguingly, the dimeric form of CD93 displayed a higher capability to interact with Multimerin-2 compared to the monomeric form, whereas no significant binding was observed to EMILIN2 (Fig. 3B). These results were further substantiated by immunoprecipitation experiments of cell extracts from migrating ECs, which confirmed a higher capability of the dimeric form of CD93 to bind to Multimerin-2 compared to the monomeric form (Fig. 3C and D).

2.3. Expression of the functional CTLD-sushi region of CD93 in prokaryotic cells

To gain molecular insights into the CD93 dimerization, we expressed the prokaryotic optimized D1X sequence (D1X-pr) in bacterial cells to obtain large amounts of pure and homogeneous protein for the subsequent biochemical analyses. Due to the presence of four disulfide bonds in the CTLD domain that are instrumental for proper folding [3], we co-expressed the pTIFA vector encoding a sulfhydryl oxidase (Erv1p) and a disulfide bond isomerase (DsbC) together with the D1X-pr plasmid in
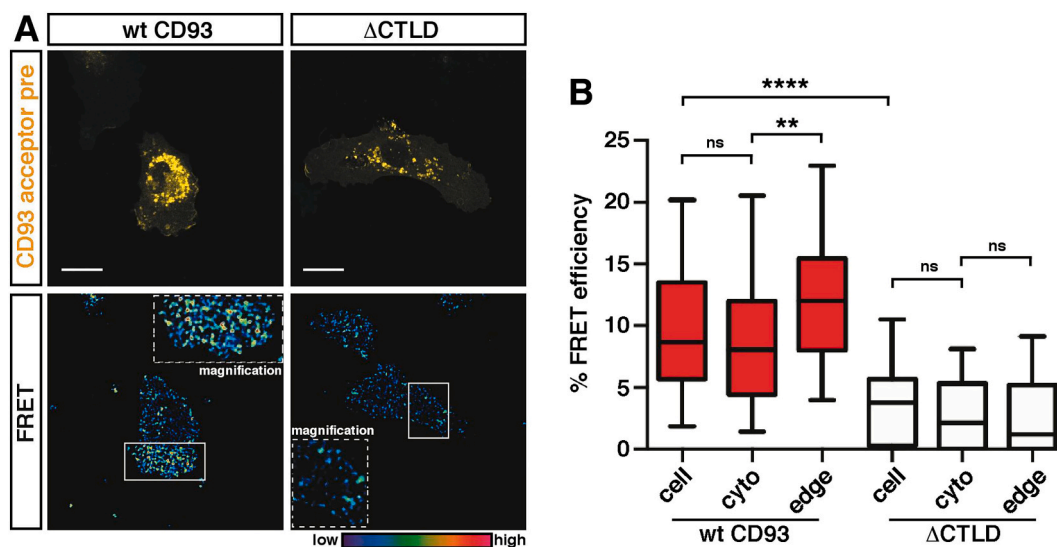

Fig. 2. CD93 dimerizes in ECs. A: FRET analysis on HUVECs transiently transfected with wild type CD93-YFP together with wild type CD93-CFP (wt CD93) or the ΔCTLD-CFP CD93 mutant (ΔCTLD). Representative confocal images of transfected migrating cells before photobleaching (acceptor pre) are shown. Scale bars, 20 μm. In the FRET images, rectangles indicate the photobleached cell area and the dashed lines the cell region used to calculate the FRET efficiency. Magnifications of the photobleached cell area are shown. The colored scale represents the color range of FRET efficiency. B: Plot showing the fluorescence increase (% FRET efficiency) upon photobleaching of migrating ECs (*n* = 44 cells for wild type CD93 and *n* = 33 cells for ΔCTLD). After photobleaching, additional ROIs, including more discrete cell regions inside the cell (cyto; *n* = 40 regions for wild type CD93 and *n* = 26 regions for ΔCTLD) or at the cell border (edge; *n* = 39 regions for wild type CD93 and *n* = 26 regions for ΔCTLD), were chosen for a more accurate evaluation of the FRET efficiency. Data are presented as box and whisker plot. ****$P < 0.0001$, **$P < 0.01$, and ns, not significant; one-way ANOVA.
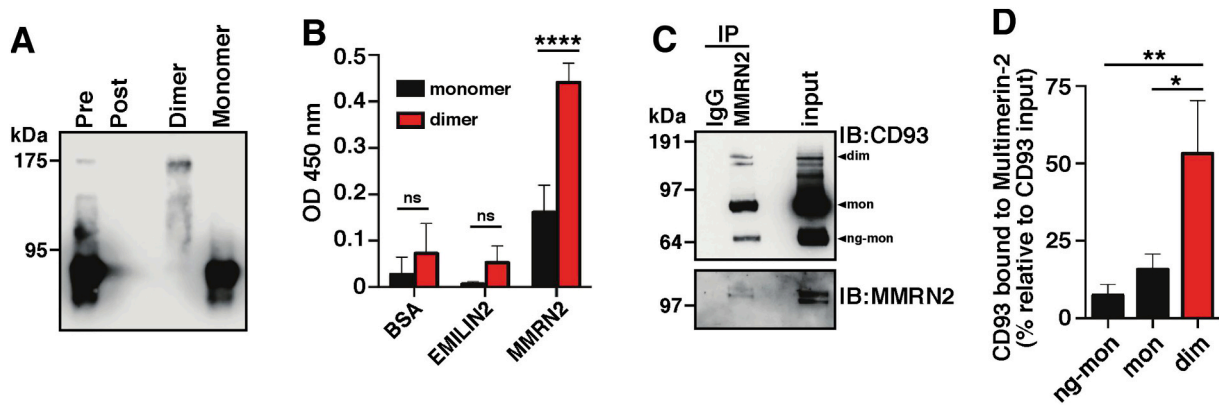
Fig. 3. Dimeric CD93 interacts with Multimerin-2. A: Western blot analysis of the pooled fractions from size exclusion chromatography of nickel-affinity purified human D1D3-His using anti-CD93 antibodies. Samples before loading (Pre) and the flow-through (Post) are indicated B: Solid phase analysis of dimeric and monomeric CD93 binding to EMILIN2 and Multimerin-2 (MMRN2). BSA was used as a control. Anti-CD93 and HRP-conjugated secondary antibodies were used to detect bound CD93. ****$P < 0.0001$ and ns, not significant; two-way ANOVA. C: Cell extracts from migrating HUVECs were immunoprecipitated (IP) using anti-Multimerin-2 (MMRN2) or unrelated goat (IgG) antibodies. Immunoprecipitates were analyzed by Western blotting (IB) with antibodies against CD93 and Multimerin-2. Arrowheads indicate dimer (dim), monomer (mon), and the non-glycosylated monomer (ng-mon) of CD93. D: Graph displaying the non-glycosylated monomeric (ng-mon), monomeric (mon), and dimeric (dim) CD93 protein levels bound to Multimerin-2 from experiments performed as in C and expressed as percentage relative to input signals. **$P < 0.01$, *$P < 0.05$, and ns, not significant; one-way ANOVA.

bacterial cells [23]. Electrophoresis under non-reducing conditions confirmed the expression of D1X-pr in the soluble fraction (Fig. 4A). The proper folding of recombinant D1X-pr was validated by comparison with the D1X-His deletion mutant expressed in HEK 293 cells. In fact, both

the fragments displayed similar band patterns in Western blot analyses using the monoclonal antibody 4E1 (Fig. 4B). Interestingly, and in accordance with a previous work on bacterial expression of CD93 CTLD [23], immunoblotting analyses indicated that D1X-pr displayed bands
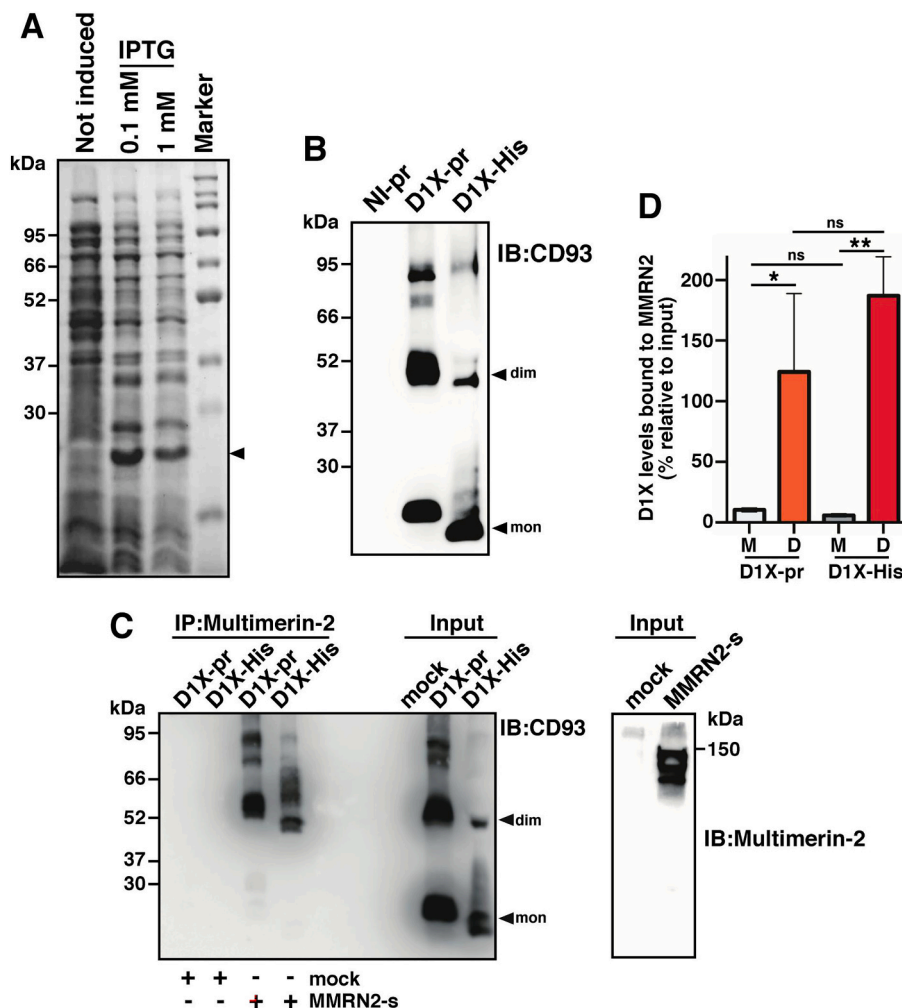

Fig. 4. The dimerization of the D1X deletion mutant facilitates the binding to Multimerin-2. A: SDS-PAGE analysis under non-reducing conditions of soluble fractions from BL21 cell lysates induced or not with IPTG as indicated. Gels were stained using the Coomassie Blue dye. An arrowhead indicates the expressed recombinant protein. B: Western blot analysis of cell lysate from prokaryotic (D1X-pr) and supernatant from eukaryotic (D1X-His) D1X-expressing cells using the anti-CD93 antibody 4E1. Arrowheads indicate the monomeric (mon) and dimeric (dim) D1X forms. NI-pr, cell lysate from bacterial cells not induced with IPTG. C: Soluble cell lysates from bacterial D1X-expressing cells (D1X-pr) or supernatants of D1X-transfected HEK 293 cells (D1X-His) were incubated with supernatants of Multimerin-2-expressing (MMRN2-s) or not (mock) HEK 293 cells and immunoprecipitated using antibodies against Multimerin-2. Immunoprecipitates were analyzed by Western blotting (IB) using anti-CD93 antibodies. Arrowheads indicate monomeric (mon) and dimeric (dim) D1X forms. Input of the mock or Multimerin-2-containing supernatants was analyzed by Western blotting using anti-Multimerin-2 antibodies. D: Quantitative analysis of D1X protein levels bound to Multimerin-2 (MMRN2) from experiments performed as in C. Values represent the percentage of monomeric (M) and dimeric (D) D1X levels bound to Multimerin-2 relative to input signals. **$P < 0.01$, *$P < 0.05$, and ns, not significant; one-way ANOVA.

double the molecular weight of the monomeric form, as observed with the deletion mutant expressed in eukaryotic cells (Fig. 4B). Peptide mapping, performed by chymotrypsin digestion of monomeric and dimeric D1X-pr bands followed by reverse-phase-ultra-HPLC-MS/MS analysis, respectively confirmed a 65 % and 47 % matching of peptides with the CD93 amino acidic sequence (Fig. S3), suggesting that after bacterial expression, D1X-pr can assume both the monomeric and dimeric status. To determine whether the D1X dimer could bind to Multimerin-2, we exogenously expressed soluble Multimerin-2 in HEK 293 cells, incubated the supernatant of Multimerin-2-transfected cells with either bacterial or mammalian-expressed D1X (D1X-pr and D1X-His, respectively), and performed co-immunoprecipitation experiments. It is noteworthy that both the prokaryotic- and eukaryotic-expressed deletion mutants interacted with Multimerin-2, and importantly, the dimeric D1X mutants showed enhanced binding to Multimerin-2 compared to the monomeric forms (Fig. 4C, quantified in 4D). Collectively, the above experimental procedures led us to obtain a bacterial-derived soluble CTLD-sushi region of CD93, which reflects key features of its counterpart expressed in eukaryotic cells. Hence, large-scale production of D1X-pr was carried out for further X-ray crystallographic studies (Fig. S4).

2.4. CD93 CTLD-sushi crystal structure

The structure of D1X-pr was obtained to 1.92 Å resolution, in the orthorhombic space group C222$_1$ (Table 1). Our initial efforts to use the

Table 1
Data collection and refinement statistics of the D1X-pr structure. Values for the outer shell are given in parentheses.

	D1X-pr mutant
PDB ID	8A59
Data collection statistics	
Diffraction source	I04 (DLS)
Wavelength (Å)	0.9795
Temperature (K)	100
Detector	Eiger2 XE 16M
Crystal-detector distance (mm)	275.4
Rotation range per image (°)	0.25
Exposure time per image (s)	0.1
Space group	C222$_1$
No. of molecules/ASU	1
a, b, c (Å)	63.71, 112.50, 73.26
Resolution range (Å)	73.26–1.92 (2.02–1.92)
Total no. of reflections	253,124 (37462)
No. of unique reflections	20,515 (2956)
Completeness (%)	100.0 (100.0)
Redundancy	12.3 (12.7)
⟨$I/\sigma(I)$⟩	12.3 (2.2)
R_{meas}	0.076 (1.278)
Overall B factor from Wilson plot (Å^2)	47.9
Refinement statistics	
Resolution range (Å)	55.50–1.92 (1.97–1.92)
No. of reflections, working set	19,418 (1392)
No. of reflections, test set	1056 (82)
Final R_{cryst}	0.21 (0.30)
Final R_{free}	0.27 (0.35)
No. of non-H atoms	
Protein	1636
Others (sulfate anion, glycerol molecule)	51 (15, 36)
Water	80
Total	1767
R.m.s. deviations	
Bonds (Å)	0.008
Angles (°)	1.569
Average B factors (Å^2)	57.3
Estimate error on coordinates based on R value (Å)	0.15
Ramachandran plot	
Most favored (%)	94.4
Allowed (%)	5.6

structures of other CTLDs as search models were unsuccessful, reasonably for their low structural conservation with CD93. However, we were able to solve the structure of D1X-pr using the CD93 CTLD-sushi structural model predicted by AlphaFold2 for the molecular replacement procedure. The structure was then refined and validated for PDB deposition under the accession code 8A59 (Table 1). Crystallographic analysis showed that the crystal asymmetric unit (ASU) contains a single protein chain, completely rebuilt from amino acid 26 to 257, except for segments 193–196 and 226–234 (Fig. 5A). Four sulfate anions and six glycerol molecules, from both precipitant and cryoprotectant solutions, and 77 water molecules further complete the crystal ASU. The CTLD (residues 1–186) folds in two antiparallel β-sheets (first layer: strands β1, β2, β3, and β9; second layer: strands β4, β5, β7, and β8) and two alpha-helices, and exhibits the peculiar folding of the canonical domain, including a "loop in a loop" structure and a hydrophobic core (Fig. 5A). The sushi-like domain (residues 187–257) has an all β-structure, being folded in two β-sheets. Strands β11, β12, β14, and β15 generate the main antiparallel layer and three shorter strands, β10, β13, and β16 define the second (Fig. 5A). The structure of D1X-pr is characterized by six intramolecular disulfide bridges spread over both protein domains. In addition to the six canonical cysteine residues that form a set of three highly conserved disulfide bridges (C31-C36, C53-C180, and C141-C165), the CTLD includes two additional cysteine residues (C104 and C136), which lie within the long-loop connecting β5, β6, and β7. These cysteine residues form a fourth disulfide bridge that locks the apical portion of this flexible long-loop region (Fig. 5A). The CTLD is packed over the sushi-like domain (residues 187–257), which shows an all β-structure (Fig. 5A). Four cysteine residues, peculiar to this domain, form two additional disulfide bridges (C188-C240 and C225-C257) that contribute to stabilize the folding.

2.5. The CTLD-sushi region of CD93 forms an antiparallel dimer

The results of the crystallographic analyses clearly showed that D1X-pr dimerizes. The partner subunit of the D1X-pr dimer is generated by binary symmetry (Fig. 5B; the whole D1X-pr crystal packing is shown in Fig. S5). The dimer halves are arranged in an antiparallel manner, with the CTLD of one subunit facing the sushi-like domain of the partner (Fig. 5B). The intersubunit contact area is thus extended over the whole D1X-pr structure, creating an interface of about 1003 Å^2. The interface area is mostly hydrophobic on both sides, whereas the central region is characterized by a hydrophilic nature (Fig. 5C). Indeed, four arginine residues (R81 and R82 of both dimer halves) are exposed on the central part of the interface area, generating a positively charged pocket in which a sulfate ion is accommodated (Fig. 5B). To validate the functional relevance of the dimeric assembly observed in the crystal structure, we attempted to build a dimer of the whole extracellular domain of CD93, using the model predicted by AlphaFold2 [24,25]. The predicted model for the CTLD and sushi-like domain agrees with the crystal structure of D1X-pr, as indicated by their structural comparison resulting in a r.m.s. deviation (r.m.s.d.) upon Cα-matching of 0.98 Å. The remaining portion of the CD93 extracellular domain is characterized by confidence prediction with the exception of the mucin-like domain. Thus, the resulting model of the CD93 dimer clearly evidences that it can be generated by the antiparallel interaction between the CTLD and the sushi-like domain of two adjacent extracellular monomers (Fig. 6), validating the functional role of the dimer observed in the crystal structure. In summary, the above results indicate that in a hydrophilic environment the CD93 receptor tends to adopt a dimeric structure, responsible for ECM-EC interactions and activation of functional signals.

3. Discussion

Dimerization plays a key role in the regulation of several transmembrane protein families. Compared to the monomeric counterpart, dimers offer the possibility of allosteric control, to expand the binding
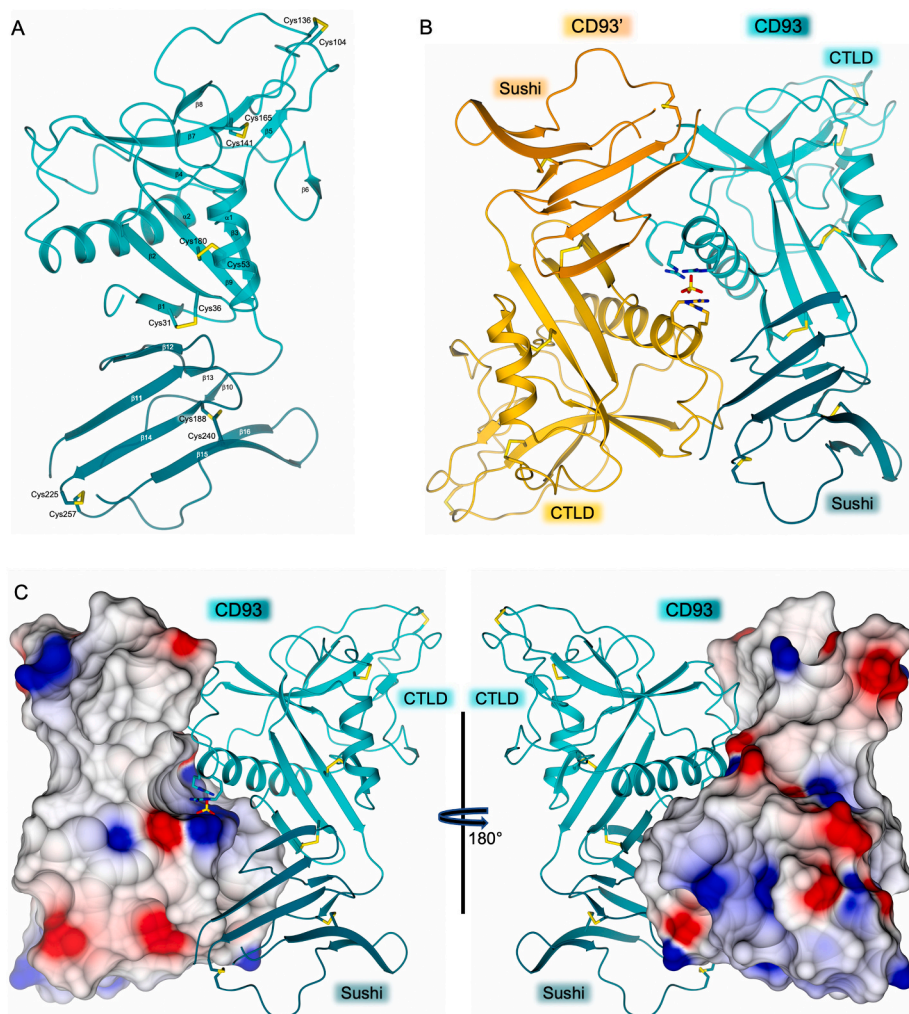
Fig. 5. Crystallographic structure of the CTLD-sushi region of CD93. A: Cartoon representation of the crystal asymmetric unit of the CTLD (cyan) and sushi-like domain (teal) of the D1X-pr deletion mutant. Cysteine residues are shown in stick and carbon atoms are color coded according to the CD93 domains. Numbered β-strands are indicated. B: Structural model of the D1X-pr dimer. In the dimer halves, the CTLDs are cyan and light orange and the sushi-like domains are teal and orange. A sulfate anion is bound to four arginine residues (R81 and R82 of both dimer halves) in the central area of the dimer interface. C: Front and back views (180° rotation on the vertical axis) of the D1X-pr dimer. One dimer half is rendered in cartoon (cyan CTLD and teal sushi-like domain) and the partner calculated by PDBePISA is shown as surface (color coded according to the local electrostatic potential). Atoms are colored in red oxygen, blue nitrogen, and yellow sulfur.

surfaces, to generate new active sites at the subunit interfaces, and to produce large interaction networks [26]. Therefore, spatial and temporal changes in oligomeric states of cell surface receptors result in a complex network of protein-protein interactions and receptor intracellular trafficking that dynamically regulate cell-signaling mechanisms. EC migration is a crucial step in both physiological and pathological angiogenesis and the cell receptor CD93 has extensively proved to be involved in its regulation. Specifically, CD93 is expressed on the EC plasma membrane and establishes appropriate cellular programs leading to vessel growth. This occurs thanks to its interaction with the ECM, funneling intracellular programs which in turn regulate the actin cytoskeleton dynamics required for a proper EC migration [8,10,13]. Despite previous analyses had suggested that CD93 could form dimers [23,27], an in-depth characterization of CD93 dimers has never been attempted in more physiological contexts. In this study, not only we demonstrate that the molecule dimerizes but also that the dimerization is instrumental to regulate its function. In fact, using classical approaches for detecting receptor-receptor interactions [28], we showed that in primary ECs CD93 dimerizes and the dimeric form, by expanding its binding surface, enhances the interaction to its physiological ligand Multimerin-2, which is usually structured as a homotrimer in the ECM [22]. Interestingly, although classical FRET methodology may entail some drawbacks [21], the use of a mutant lacking the CTLD together with the wild type protein allowed us to measure the CD93 association in migrating ECs and to highlight the key role played by the CTLD in the dimerization of CD93.

The first crystal structure resolution of the CTLD-sushi region of a CTLD group 14 family member shed new light on the CD93/Multimerin-2 interaction. The disulfide bridge formed in the CTLD by two non-canonical cysteine residues (C104 and C136) is crucial to shape the long-loop surface necessary for the binding of CD93 to Multimerin-2. Indeed, the mutation of these two cysteine residues inhibits the binding to Multimerin-2 without affecting the CD93 folding [13]. Importantly, the sushi domain is an extracellular motif that can contribute to protein-protein interactions [29]. However, until now its structural role in the CD93 receptor was unknown. Here we found that the sushi-like domain of CD93 exerts a pivotal contribution in dimer formation and, consequently, in the binding to Multimerin-2. The comparison of CD93 CTLD structure with that of the CTLD group 5 family member CD69 [30], showed that CD69 shares with CD93 the conserved structural features, peculiar to the CTLD (Fig. 7A and B). The isolated CD69 CTLD is known to dimerize and to adopt a parallel arrangement (Fig. 7D). Although the isolated CD93 CTLD may also share this propensity, our results showed that the sushi-like domain directly interacts with the CTLD of the partner subunit and shares multiple contacts across the monomer-monomer interface (Fig. 7C). Of note, the sushi-like domain is crucial to achieve a functional status for the interaction with Multimerin-2, as point mutations in the sushi-like domain of CD93 have been shown to destabilize the CD93/Multimerin-2 interaction and to hamper EC migration [4]. Furthermore, the group 14 CTLD members CD93, CLEC14A, and CD248 directly bind to Multimerin-2 and only thrombomodulin does not [13]. Intriguingly, due to the lack of four conserved cysteine residues, thrombomodulin is the only family member that does not incorporate a structured sushi-like domain [5].
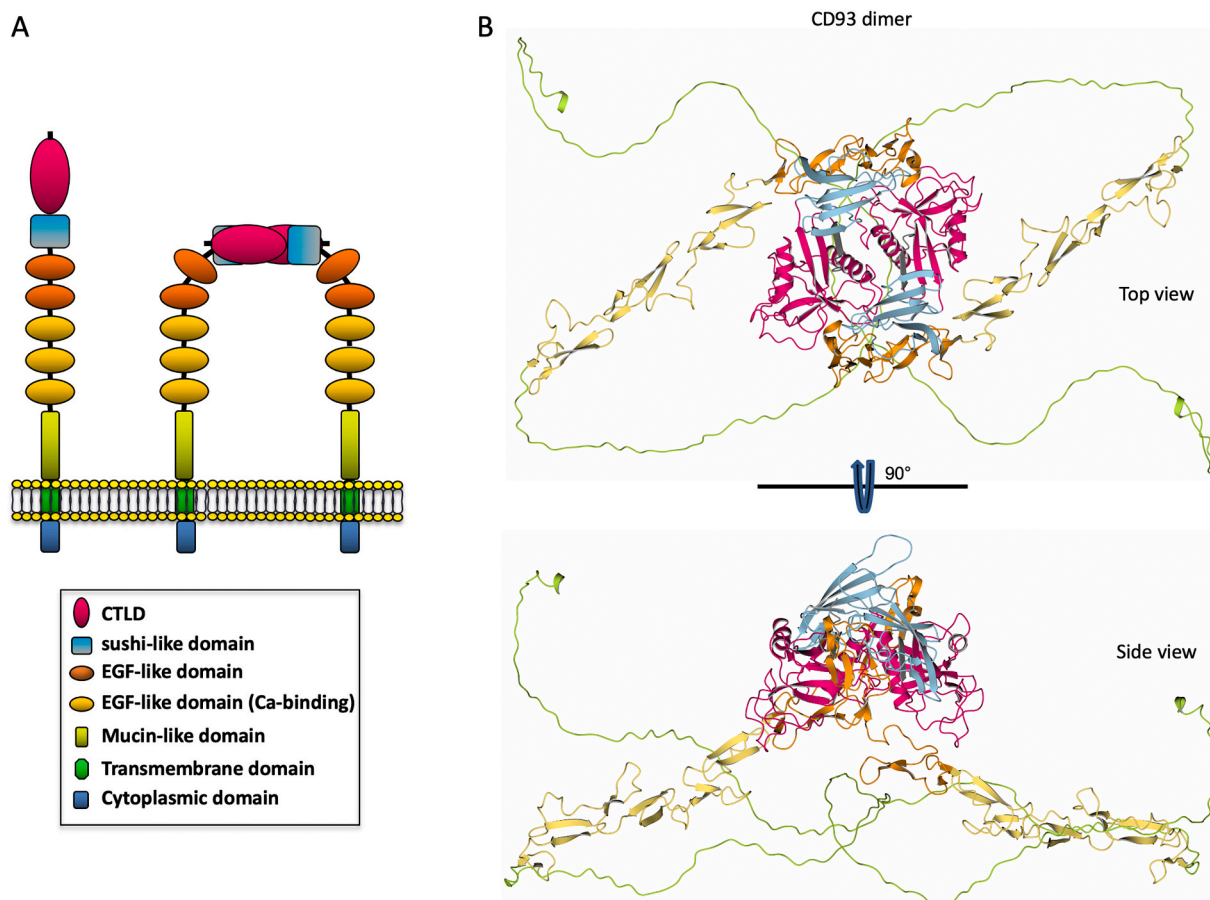
Fig. 6. Structural model of CD93 dimerization. A: Schematic representation of the antiparallel CD93 dimerization, a mechanism relying on recognition and binding of the CTLD and the sushi-like domain. The CD93 domains are colored according to the legend. B: Top and side view of the structural model of the antiparallel CD93 dimer. The structural model of each CD93 unit was generated with AlphaFold2 considering only the extracellular domains of CD93. Domains are color-coded according to the legend of panel A. The CD93 dimer was built by structural superimposition of the CTLD and sushi-like domain of each unit with those observed in the crystal structure of the D1X-pr dimer. Regions including the CTLD and sushi-like domain were validated by the crystal structure of D1X-pr. The EGF-like repeats are confident prediction structures, whereas the mucin-like domain is very-low confidence.

The antiparallel arrangement adopted by D1X-pr results in a quite peculiar shape of the surface area, remarkably different from the one observed in the CTLD dimer of CD69 (Fig. 7C and D). Therefore, our results support a working model in which the N-terminal domain of each CD93 monomer is bent, allowing the formation of antiparallel dimers kept together by CTLD-sushi interactions (Fig. 6). Structural matching of the CTLD and the sushi-like domain with the crystal structure of the D1X-pr dimer enabled the generation of a structural model of the whole CD93 receptor, showing the tilting of the N-terminal regions, in which the CTLD and the sushi domain of distinct monomers interact with each other (Fig. 6). The presence of flexible interconnecting regions between the CTLD-sushi region and the EGF-like repeats suggests the ability of these regions to bend and rearrange, allowing the formation of an antiparallel dimer, as observed in the crystal structure of D1X-pr.

Intriguingly, we cannot currently rule out the possibility that the N-terminal region of CD93 may form cell-interactions and/or heterodimers with other C-type lectin XIV family members, which all interact with ECM proteins and support EC adhesion and migration [5]. If this was the case, heterodimer formation might expand the ways of protein regulation by creating new binding surfaces, active sites, or protein interaction networks. Consistent with this assumption, the CTLDs of thrombomodulin and CLEC14A have been implicated in cell-cell interaction and blocking intermolecular interaction of thrombomodulin and CLEC14A using anti-CTLD antibodies was shown to inhibit the EC function [31,32]. Undoubtedly, the resolution of the three-dimensional structure of the other protein family members will provide further molecular and functional insights into this transmembrane receptor family.

In the last decade, the scientific community has pointed towards vascular remodeling in the attempt to normalize the tumor vasculature and improve cancer treatment [33]. Ideally, instead of starving the tumor by vascular pruning, the normalization of the disorganized tumor vessels would improve tumor perfusion, promote drug delivery, and provide a less hostile environment for immune cell infiltration and function. However, if for cancer treatment this seems to be the main road to follow, for neovascular pathologies such as age-related macular degeneration the most promising strategy still entails vessel pruning to prevent exudation and halt the progression of the disease [34]. Therefore, the strategies aimed at targeting the vessels are context-dependent and may differ according to the different pathologies. In this scenario, CD93 represents an ideal target. Indeed, being expressed mainly in the activated endothelium, CD93 neutralization should minimize unwanted side effects and has already shown the potential flexibility for anti-angiogenic therapy as well as vascular normalization [15,35].

4. Materials and methods

4.1. DNA constructs

The *CD93* full-length cDNA (GenBank accession number NM_012072.4) cloned into pcDNA3 vector, the chimeric construct expressing human CD93 fused to YFP, the chimeric constructs expressing the Myc-tagged extracellular domains of CD93, and the vector
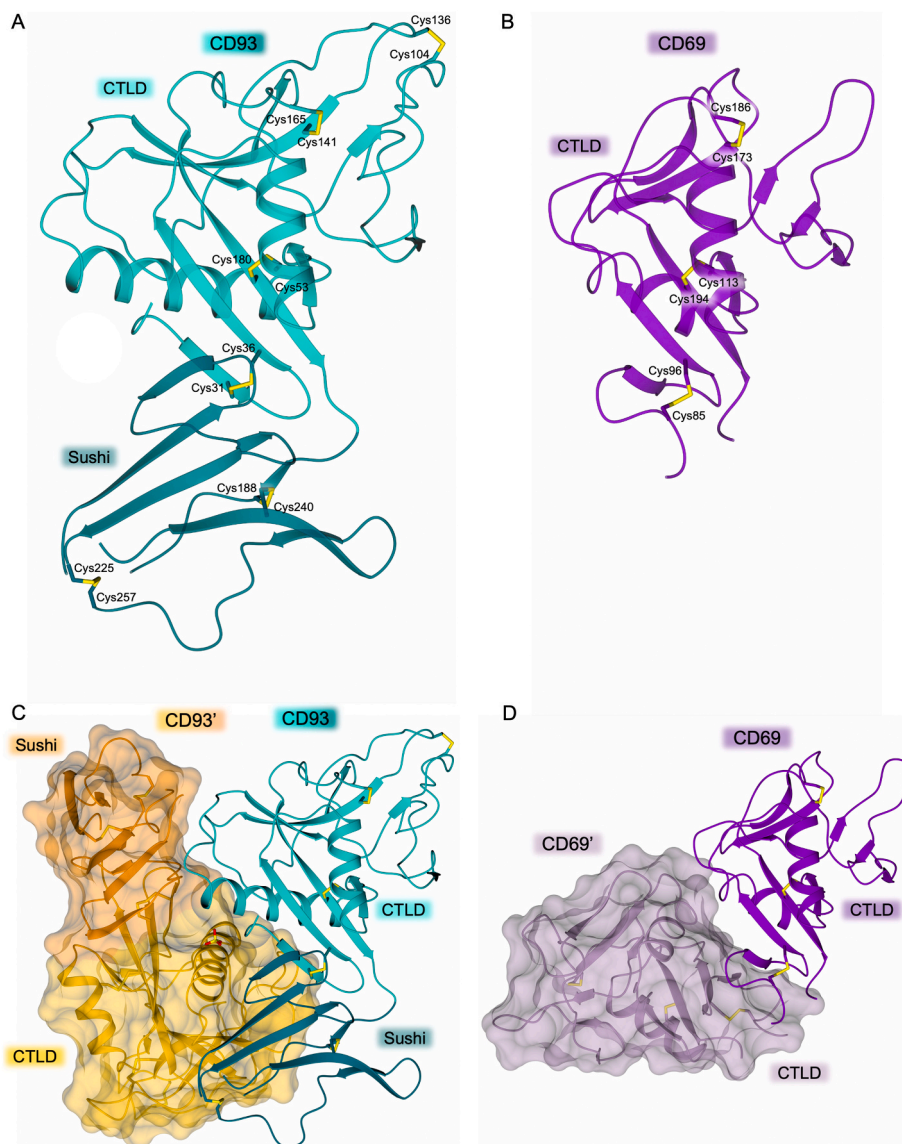
Fig. 7. Structural comparison between CD93 and CD69. Cartoon representation of (A) D1X-pr (cyan CTLD and teal sushi-like domain) and (B) CD69 (purple CTLD). Disulfide bridges are in sticks. C: CTLDs (cyan and light orange) and sushi-like domains (teal and orange) of D1X-pr in the dimeric conformation. A sulfate anion is shown. D: Dimeric structure formed by the CTLDs (purple and lilac) of CD69. In C and D, one dimer half is displayed as transparent surface.

expressing Multimerin-2 were generated as previously described [7,36]. The Myc-tagged D1X-TM construct expressing the membrane bound CTLD-sushi domains (covering the amino acid residues from 1 to 257 of the human CD93 sequence, UniProKB accession number Q9NPY3), fused to the transmembrane domain (TM, covering the amino acid residues from 581 to 605 of the human CD93 sequence) was obtained by PCR amplification of the CD93 TM cDNA, using the following primers: For1, 5′-GTTCGACTGGGGCAGCTCGGGCCCCCTCTGTGGATCCCATCTG CTTTTATTCTACATCCTAGGCACC-3′ and Rev1, 5′-GTCCTCTTCAGAA ATGAGCTTTTGCTCCATAGCTTTAAATAGATCTGCGACCAGTAGCCCC AGAGCC-3′. The PCR fragment was assembled into the *Avr*II digested Myc-tagged pCS2-D1X vector [7], using the NEBuilder HiFi DNA assembly cloning kit (New England Biolabs, Ipswich, MA, USA). D1X-TM fused to Myc tag was subcloned into a third generation self-inactivating (SIN) lentiviral vector (System Biosciences, Palo Alto, CA, USA) under the control of elongation factor-1 alpha (EF1α) promoter, to generate the vD1X-TM construct. The deletion mutant lacking the amino acid residues from 25 to 180 of the human CD93 sequence (ΔCTLD), was obtained by PCR amplification, using the following primers: For2, 5′-GAGAGGATCCAAGTTCAGCTTCAAAGGCAT-3′ and Rev2, 5′-

GAGATCTAGATCAGCAGTCTGTCCCAGGT-3′. The PCR fragment was cloned into pCS2 vector containing the signal peptide of the human CD93 sequence (Fig. 1C) [7]. For FRET analysis, the full-length cDNA of human *CD93* and the ΔCTLD sequence were subcloned into pECFP-N1 vector (Takara Bio Inc., Kasatsu, Japan), positioning the fluorescence tag at the C-terminus. The D1D3-His and D1X-His constructs, for eukaryotic expression of the CD93 fragments (covering the amino acid residues from 1 to 580 and 1 to 257 of the human CD93 sequence, respectively) fused to His6x tag, were generated by replacing the Myc tag with the His6x tag in the pCS2-D1D3 and pCS2-D1X vectors [7]. All constructs were checked by sequencing. The D1X-pr construct, containing the CTLD-sushi sequence of human CD93, optimized for prokaryotic expression and cloned into pET-28a vector, was purchased from GenScript (Piscataway, NJ, USA). The pTIFA vector, encoding the Erv1p and DsbC enzymes useful for disulfide bridge formation and proper folding of heterologous proteins expressed in *E. coli*, was kindly provided by Dr. W. Viranaicken (UMR PIMIT, France).

4.2. Cell culture and transfection

HUVECs from single donors were purchased from PromoCell (Heidelberg, Germany) and grown on gelatin-coated plates in antibiotic-free Endothelial Cell Basal Medium (EBM-MV2) with supplements (Promo-Cell) as previously described [37]. For lentivirus production, human Lenti-X 293T cells (Takara Bio Inc) were grown in DMEM containing 2 % FBS and 1 mM sodium butyrate (Merck KGaA, Darmstadt, Germany) to increase viral titer [38]. Transient transfection of HEK 293 cells (Merck KGaA) was performed using the Transporter 5® Transfection Reagent (Polysciences, Warrington, PA, USA), following manufacturer's instructions. Transient transfection of HUVECs was performed by electroporation as previously reported [11]. 24 h after transfection, transfected cells were detached from the culture plate by a non-enzymatic-method and let them migrate for 3 h before analysis [8].

4.3. Antibodies

The following primary antibodies were used: mouse monoclonal anti-CD93 (clone 4E1) [7]; rabbit anti-CD93 (HPA009300, Atlas Antibodies, Bromma, Sweden); mouse monoclonal anti-CD93 (clone mNI-11, MBL International, Woburn, MA, USA); rabbit anti-GAPDH (ab9485) and rabbit anti-Myc (ab9106, Abcam, Cambridge, United Kingdom); rabbit anti-Multimerin-2 [39]; goat anti-Multimerin-2 (sc-54120, Santa Cruz Biotechnology, Dallas, TX, USA); goat IgG isotype control (02-6202, Thermo Fisher Scientific, Waltham, MA, USA).

4.4. Immunoprecipitation and immunoblotting analysis

Co-immunoprecipitation experiments were carried out using the protein A-conjugated dynabeads (Thermo Fisher Scientific) according to the manufacturer's instructions. Cell lysates were immunoprecipitated using the primary antibody and analyzed by immunoblotting as previously described [40]. Under non-reducing conditions, protein samples were not boiled nor reducing additives were added prior to SDS-PAGE. Analysis of native proteins was performed using NativePAGE Bis-Tris 4–16 % polyacrylamide gels (Thermo Fisher Scientific). Supernatants containing the deletion mutants were loaded using the NativePAGE SDS-free and non-reducing sample buffer. Electrophoresis was carried out accordingly to the manufacturer's instructions and proteins were analyzed by immunoblotting. To compare protein levels of different samples, densitometric analysis was performed using the gel analyzer tool of ImageJ2.

4.5. Flow cytometry

Flow cytometry analysis was performed as previously described with slight modifications [16]. Briefly, transiently transfected HEK 293 cells were detached from the culture plate using a non-enzymatic method, incubated with anti-CD93 antibodies followed by appropriate Alexa Fluor 488-labelled secondary antibodies, and analyzed on CytoFLEX LX flow cytometer equipped with CytExpert 2.4 software (Beckman Coulter Life Science, Indianapolis, IN, USA). Data were processed using FlowJo version 10.8.1 (FlowJo, Ashland, OR, USA).

4.6. FRET analysis

Transfected HUVECs were fixed in 4 % paraformaldehyde, washed with quenching solution (50 mM Tris-HCl/100 mM NaCl), and mounted in Fluoramount G medium (Thermo Fisher Scientific). FRET experiments were carried out using a Leica TCS SP8 AOBS confocal laser-scanning microscope, following the TCS SP8 and FRET AB manufacturer's software. A Leica HC PL APO 63x/1.30 Glyc CORR CS2 glycerol objective was used for the acquisition of images. Images (512 × 512 pixel resolution) were acquired at a scan speed of 400 Hz image lines/s. Confocal scanner configuration was set as follows: pinhole at 1.4 Airy

units, line averaging function at 2, and bidirectional phase X at −30.95. FRET acceptor photobleaching (apFRET) analyses were performed by setting the diode laser 405 at 2.5 % and general argon laser intensity at 60 %. For proper image recording, hybrid detectors HyD were employed by gating a spectral acquisition window of 436–505 nm for the donor (CFP) and 524–600 nm for the acceptor (YFP). In the photobleaching procedure, cells were bleached using the 514 nm argon laser beam at 100 % intensity until the acceptor was photobleached down to about 10 % of its initial value. FRET analysis was performed using ImageJ2 and the FRETcalc plug-in. FRET efficiency was calculated as previously described [41,42].

4.7. Protein expression and purification

To produce on large scale the soluble extracellular domain of CD93, adherent HEK 293 cells growing in 175-cm^2 culture flasks were transfected with the D1D3-His construct. 24 h after transfection, cells were washed with PBS and EX-CELL 293 serum-free medium (Merck KGaA), containing 6 mM L-Glutamine and 1 mM sodium butyrate, was added. A total of 1250 mL of cell supernatant was harvested from 20 culture flasks at days 2 and 3 after transfection. The harvested supernatant was centrifuged to remove the cell debris and purified by nickel-affinity chromatography. The purified D1D3-His protein was concentrated to 0.5 mg/mL and 2 mL of protein solution were subjected to size exclusion chromatography on a HiLoad 16/600 Superdex 200 pg preparative SEC column (Cytiva, Marlborough, MA, USA). Fractions were next analyzed by Western blotting under non-reducing conditions using anti-CD93 antibodies. To express the prokaryotic D1X protein (D1X-pr), BL21 (DE3) *E. coli* cells were transformed with the D1X-pr and pTIFA vectors and selected in agar plates as previously described [23]. Single colonies were pre-inoculated in 20 mL of LB medium containing 25 μg/mL kanamycin and 35 μg/mL chloramphenicol and grown overnight at 37 °C with vigorous shaking. D1X-pr over-expression was obtained in 1 L of LB medium without antibiotics after 24 h of induction at 18 °C in the presence of 0.25 mM IPTG when the OD$_{600}$ reached values between 0.4 and 0.5. Cells, harvested by centrifugation, were resuspended in PBS containing 25 mM imidazole and lysozyme (0.5 mg/mL), and disrupted by sonication. After centrifugation at 11,000 ×g for 1 h at 4 °C, samples of total extract, supernatant, and pellet were analyzed by SDS-PAGE under reducing conditions followed by Coomassie staining (SimplyBlue SafeStain, Thermo Fisher Scientific) to check recombinant protein expression.

Protein purification was performed using a fast protein liquid chromatograph (FPLC) Akta purifier system endowed of a UV-900 Detector and a Frac-900 fraction collector (GE Healthcare, Chigago, IL, USA). Nickel-affinity chromatography was carried out in a HisTrap FF 5 mL column (Cytiva), using a step-gradient elution protocol and imidazole as a competitive agent. Protein elution was achieved at imidazole concentrations ranging from 40 to 125 mM. Fractions containing the target protein were identified by SDS-PAGE under reducing conditions, pooled, and extensively dialyzed in PBS. The His-tag cleavage of the D1X-pr protein was performed during the dialysis by adding directly inside the membrane an in-house produced TEV protease (0.05 mg/mg of target protein). After an overnight incubation, the tag cleavage was almost complete (>98 %, verified by SDS-PAGE), and the mature protein was subjected to a second round of nickel-affinity chromatography. The effective tag removal was confirmed by SDS-PAGE under reducing conditions and Coomassie staining. Finally, after dialysis in PBS, protein concentration was measured using the bicinchoninic protein assay kit (EuroClone, Pero, Mi, Italy).

4.8. ELISA-based solid-phase binding assay

96-well Maxisorp plates (Nunc, Roskilde, Denmark) were coated (150 ng/well) with the following adhesive substrates: bovine serum albumin (Sigma-Aldrich, Saint Louis, MO, USA), human EMILIN2 [43],

and human Multimerin-2 [39]. The plates were blocked with bovine serum albumin prior to the addition of the purified monomeric or dimeric D1D3-His protein at 100 ng/well. The plates were then washed with PBS and anti-CD93 antibodies were added to the wells. After PBS washing, HRP-conjugated secondary antibodies were used to detect bound CD93. *o*-Phenylenediamine (Sigma-Aldrich) HRP substrate was used to assess color development. The optical density values were measured using EnVision 2105 multimode plate reader (Perkin Elmer, Waltham, MA, USA).

4.9. Peptide mass fingerprint analysis

The nickel-affinity purified D1X-pr protein was separated on a 4 to 12 % gradient SDS-PAGE gel under non-reducing conditions. Coomassie blue-stained gel bands were excised, de-stained, reduced, alkylated, and digested by chymotrypsin (Promega, Madison, WI, USA). The resulting peptides, desalted, dehydrated, and reconstituted in 0.1 % formic acid in water, were analyzed using RP-UHPLC-MS/MS. The peptide separation was performed at 35 °C on a PepMap RSLC C18 100 Å column (0.075 × 150 mm, 3 μm, Thermo Fisher Scientific) and the analysis was carried out using a gradient elution (phase A: 0.1 % formic acid in water; phase B: 0.1 % formic acid in acetonitrile) at a flow rate of 0.3 mL/min. The mass spectra were acquired using a Q-Exactive HF-X Orbitrap mass spectrometer (Thermo Fisher Scientific) in "data-dependent scan" mode, able to acquire both the full mass spectra in high resolution and to isolate and fragment the twenty ions with highest intensity present in the mass spectrum. The raw data obtained were analyzed using the Biopharma Finder 2.1 software (Thermo Fisher Scientific). The elaboration process consisted in the comparison between the peak list obtained in silico simulating protein digestion of CD93 and the experimental data.

4.10. Crystallization

The recombinant mature D1X-pr was concentrated to 3.81 mg/mL in PBS and 2 mL of protein solution were subjected to size exclusion chromatography on a HiLoad 16/600 Superdex 75 pg preparative SEC column (Cytiva). Fractions were analyzed by immunoblotting using anti-CD93 antibodies. The recombinant mature D1X-pr was concentrated to 7.85 mg/mL in 20 mM TRIS, pH 7.2 and directly used for crystallization trials using the vapor diffusion sitting drop technique at room temperature [44]. More than 100 different crystallization solutions from commercially available kits of Hampton Research (Aliso Viejo, CA, USA) and Jena Bioscience (Jena, Germany) were screened as precipitant solutions. Drops consisting of 1 μL protein solution and 1 μL precipitant were equilibrated against a 200 μL reservoir. Within few days of incubation at room temperature, crystal growth was observed in several conditions, all including ammonium and/or lithium sulfate as precipitants. Crystals suitable for diffraction were obtained using a precipitant solution composed of 1.0 M ammonium sulfate, 0.5 M lithium sulfate, and 0.1 M HEPES, pH 7.5. Prior to flash freezing in liquid nitrogen, crystals were singularly transferred to the cryoprotectant solutions prepared by adding 20 % vol/vol of either glycerol or ethylene glycol to the precipitant.

4.11. Data collection, structure solution, and refinement

X-ray diffraction data were collected on D1X-pr crystals using synchrotron radiation at the Diamond Light Source (DLS, Didcot, UK) beamline I04. Reflections were integrated using XDS [45] and scaled with SCALA [46] from the CCP4 suite [47]. Molecular replacement was performed using the software MOLREP [48]. The structure of the CD69 CTLD (PDB 1E87 [30]), having the highest sequence identity with CD93 (28 %), was initially used as a search model, but no acceptable solutions were obtained from the molecular replacement procedure. However, the use of the structure obtained from the AlphaFold2 predicted model CTLD-sushi-AF (see below) allowed us to obtain a starting structural model of D1X-pr. Next, the structure was refined using REFMAC5 [49] from the CCP4 suite. The molecular graphic software Coot was used for manual rebuilding and modeling of missing atoms in the electron density and to add solvent molecules [50]. The final model of recombinant mature D1X-pr was manually inspected and checked with Coot and PROCHECK [51]. The dimer interface area of D1X-pr was analyzed using the PDBePISA tool [52]. Structural figures were generated using the molecular graphic software CCP4mg [53]. Data collection, processing and refinement statistics are summarized in Table 1. Final coordinates and structure factors were deposited in the Protein Data Bank (PDB) under the code 8A59.

4.12. Generation of a functional dimerization model for full-length CD93

The structural model for human CD93 (AF-Q9NPY3-F1) was obtained using AlphaFold2 (AlphaFold Monomer 2.0) [24,25]. The first 21 N-terminal amino acid residues of the signal peptide were removed from the predicted model. The confidence of the predicted model was analyzed using the per-residue pseudo-B factors corresponding to 100-(per-residue confidence (pLDDT)) [24,25]. The region containing the CTLD and sushi-like domain (22–257) has 78.7 % residues showing a confidence/very confidence prediction, whereas only 18.7 % and 2.6 % residues are characterized by a low and very low confidence prediction, respectively. Segments containing residues with low/very low confidence prediction (22–26, 82–89, 105–110, 118–122, 130–135, 149–155, 171–173, and 227–234) were removed from the model. The resulting model was used as searching model for the structure solution by molecular replacement. The region of the CD93 predicted model containing the five EGF-like repeats (260–301, 302–344, 345–384, 384–426, and 427–468) is characterized by 90.4 % residues showing a confidence/very confidence prediction and only 9.6 % low confidence residues, suggesting a reliable structural model for this region. The mucin-like domain (470–580) shows a very low predicted confidence. The model is completed by the transmembrane helix (581–601), characterized by a very confidence prediction, and the cytoplasmic domain (602–652), which has instead a poorly predicted structure (low/very low confidence prediction for residues 616–652). The predicted model for the dimerization of the CD93 extracellular domains was generated by the superimposition of two AlphaFold2-generated structural models with the crystal structure of the D1X-pr dimer.

4.13. Statistical analysis

Data analyses were performed using Prism statistical software (GraphPad, San Diego, CA, USA) and the values represent the mean ± SD obtained from at least three independent experiments. Statistical differences among groups were analyzed using one-way ANOVA or two-way ANOVA followed by Tukey's or Sidak's multiple comparison tests, respectively. All P values reported were two-tailed and P less or equal to 0.05 was considered statistically significant.

CRediT authorship contribution statement

Conceptualization, S.B. and M.O.; methodology, S.B., L.T., and C.P.; validation, C.P. and M.O.; investigation, S.B., L.R., G.T. and L.T.; resources, A.S., F.G., F.P., A.D., C.P., and M.O.; data curation, S.B., G.T., and C.P.; writing—original draft preparation, S.B. and M.O.; writing—review & editing, G.M.T., A.D., F.G., M.M., F.P, and A.S.; visualization, M.O.; supervision, C.P. and M.O.; funding acquisition, G.M.T., A.D., F.G., A.S., M.M., and M.O.

Declaration of competing interest

The authors declare that there are no conflicts of interest.

Acknowledgements

Appendix A. Supplementary data

Supplementary data to this article can be found online at https://doi.org/10.1016/j.ijbiomac.2022.10.136.

References

[1] P. Carmeliet, Angiogenesis in health and disease, Nat. Med. 9 (2003) 653–660.

[2] B. Sennino, D.M. McDonald, Controlling escape from angiogenesis inhibitors, Nat. Rev. Cancer 12 (2012) 699–709.

[3] A.N. Zelensky, J.E. Gready, The C-type lectin-like domain superfamily, FEBS J. 272 (2005) 6179–6217.

[4] F. Galvagni, F. Nardi, O. Spiga, A. Trezza, G. Tarticchio, R. Pellicani, E. Andreuzzi, E. Caldi, P. Toti, G.M. Tosi, A. Santucci, R.V. Iozzo, M. Mongiat, M. Orlandini, Dissecting the CD93-multimerin 2 interaction involved in cell adhesion and migration of the activated endothelium, Matrix Biol. 64 (2017) 112–127.

[5] K.A. Khan, J.L. McMurray, F. Mohammed, R. Bicknell, C-type lectin domain group 14 proteins in vascular biology, cancer and inflammation, FEBS J. 286 (2019) 3299–3332.

[6] E. Langenkamp, L. Zhang, R. Lugano, H. Huang, T.E.A. Elhassan, M. Georganaki, W. Bazzar, J. Lööf, G. Trendelenburg, M. Essand, F. Pontén, A. Smits, A. Dimberg, Elevated expression of the C-type lectin CD93 in the glioblastoma vasculature regulates cytoskeletal rearrangements that enhance vessel function and reduce host survival, Cancer Res. 75 (2015) 4504–4516.

[7] M. Orlandini, F. Galvagni, M. Bardelli, M. Rocchigiani, C. Lentucci, F. Anselmi, A. Zippo, L. Bini, S. Oliviero, The characterization of a novel monoclonal antibody against CD93 unveils a new antiangiogenic target, Oncotarget 5 (2014) 2750–2760.

[8] S. Barbera, R. Lugano, A. Pedalina, M. Mongiat, A. Santucci, G.M. Tosi, A. Dimberg, F. Galvagni, M. Orlandini, The C-type lectin CD93 controls endothelial cell migration via activation of the Rho family of small GTPases, Matrix Biol. 99 (2021) 1–17.

[9] J. Du, Q. Yang, L. Luo, D. Yang, C1qr and C1qrl redundantly regulate angiogenesis in zebrafish through controlling endothelial Cdh5, Biochem. Biophys. Res. Commun. 483 (2017) 482–487.

[10] R. Lugano, K. Vemuri, D. Yu, M. Bergqvist, A. Smits, M. Essand, S. Johansson, E. Dejana, A. Dimberg, CD93 promotes β1 integrin activation and fibronectin fibrillogenesis during tumor angiogenesis, J. Clin. Invest. 128 (2018) 3280–3297.

[11] F. Galvagni, F. Nardi, M. Maida, G. Bernardini, S. Vannuccini, F. Petraglia, A. Santucci, M. Orlandini, CD93 and dystroglycan cooperation in human endothelial cell adhesion and migration, Oncotarget 7 (2016) 10090–10103.

[12] S. Barbera, L. Raucci, R. Lugano, G.M. Tosi, A. Dimberg, A. Santucci, F. Galvagni, M. Orlandini, CD93 signaling via Rho proteins drives cytoskeletal remodeling in spreading endothelial cells, Int. J. Mol. Sci. 22 (2021) 12417.

[13] K.A. Khan, A.J. Naylor, A. Khan, P.J. Noy, M. Mambretti, P. Lodhia, J. Athwal, A. Korzystka, C.D. Buckley, B.E. Willcox, F. Mohammed, R. Bicknell, Multimerin-2 is a ligand for group 14 family C-type lectins CLEC14A, CD93 and CD248 spanning the endothelial pericyte interface, Oncogene 36 (2017) 6097–6108.

[14] R. Pellicani, E. Poletto, E. Andreuzzi, A. Paulitti, R. Doliana, D. Bizzotto, P. Braghetta, R. Colladel, G. Tarticchio, P. Sabatelli, F. Bucciotti, G. Bressan, R.V. Iozzo, A. Colombatti, P. Bonaldo, M. Mongiat, Multimerin-2 maintains vascular stability and permeability, Matrix Biol. 87 (2020) 11–25.

[15] Y. Sun, W. Chen, R.J. Torphy, S. Yao, G. Zhu, R. Lin, R. Lugano, E.N. Miller, Y. Fujiwara, L. Bian, L. Zheng, S. Anand, F. Gao, W. Zhang, S.E. Ferrara, A. E. Goodspeed, A. Dimberg, X.-J. Wang, B.H. Edil, C.C. Barnett, R.D. Schulick, L. Chen, Y. Zhu, Blockade of the CD93 pathway normalizes tumor vasculature to facilitate drug delivery and immunotherapy, Sci. Transl. Med. 13 (2021), eabc8922.

[16] S. Barbera, F. Nardi, I. Elia, G. Realini, R. Lugano, A. Santucci, G.M. Tosi, A. Dimberg, F. Galvagni, M. Orlandini, The small GTPase Rab5c is a key regulator of trafficking of the CD93/Multimerin-2/β1 integrin complex in endothelial cell adhesion and migration, Cell Commun. Signal. 17 (2019) 55.

[17] M. Zhang, S. Bohlson, M. S., A. Dy, J. Tenner, Modulated interaction of the ERM protein, moesin, with CD93, Immunology 115 (2005) 63–73.

[18] W. Tong, G. Wang, L. Zhu, Y. Bai, Z. Liu, L. Yang, H. Wu, T. Cui, Y. Zhang, Pan-cancer analysis identified CD93 as a valuable biomarker for predicting patient prognosis and immunotherapy response, Front. Mol. Biosci. 8 (2022), 793445.

[19] Z. Zhang, M. Zheng, Q. Ding, M. Liu, CD93 correlates with immune infiltration and impacts patient immunotherapy efficacy: a pan-cancer analysis, Front. Cell Dev. Biol. 10 (2022), 817965.

[20] G.M. Tosi, E. Caldi, B. Parolini, P. Toti, G. Neri, F. Nardi, C. Traversi, G. Cevenini, D. Marigliani, E. Nuti, T. Bacci, F. Galvagni, M. Orlandini, CD93 as a potential target in neovascular age-related macular degeneration, J. Cell. Physiol. 232 (2017) 1767–1773.

[21] V. Fernández-Dueñas, J. Llorente, J. Gandía, D.O. Borroto-Escuela, L.F. Agnati, C. I. Tasca, K. Fuxe, F. Ciruela, Fluorescence resonance energy transfer-based technologies in the study of protein–protein interactions at the cell surface, Methods 57 (2012) 467–472.

[22] A. Colombatti, P. Spessotto, R. Doliana, M. Mongiat, G. Bressan, G. Esposito, The EMILIN/multimerin family, Front. Immunol. 2 (2012) 93.

[23] B. Nativel, A. Figuester, J. Andries, C. Planesse, J. Couprie, P. Gasque, W. Viranaicken, T. Iwema, Soluble expression of disulfide-bonded C-type lectin like domain of human CD93 in the cytoplasm of Escherichia coli, J. Immunol. Methods 439 (2016) 67–73.

[24] J. Jumper, R. Evans, A. Pritzel, T. Green, M. Figurnov, O. Ronneberger, K. Tunyasuvunakool, R. Bates, A. Žídek, A. Potapenko, A. Bridgland, C. Meyer, S.A. A. Kohl, A.J. Ballard, A. Cowie, B. Romera-Paredes, S. Nikolov, R. Jain, J. Adler, T. Back, S. Petersen, D. Reiman, E. Clancy, M. Zielinski, M. Steinegger, M. Pacholska, T. Berghammer, S. Bodenstein, D. Silver, O. Vinyals, A.W. Senior, K. Kavukcuoglu, P. Kohli, D. Hassabis, Highly accurate protein structure prediction with AlphaFold, Nature 596 (2021) 583–589.

[25] M. Varadi, S. Anyango, M. Deshpande, S. Nair, C. Natassia, G. Yordanova, D. Yuan, O. Stroe, G. Wood, A. Laydon, A. Žídek, T. Green, K. Tunyasuvunakool, S. Petersen, J. Jumper, E. Clancy, R. Green, A. Vora, M. Lutfi, M. Figurnov, A. Cowie, N. Hobbs, P. Kohli, G. Kleywegt, E. Birney, D. Hassabis, S. Velankar, AlphaFold protein structure database: massively expanding the structural coverage of protein-sequence space with high-accuracy models, Nucleic Acids Res. 50 (2022) D439–D444.

[26] Y. Liu, D. Eisenberg, 3D domain swapping: as domains continue to swap, Protein Sci. 11 (2002) 1285–1299.

[27] Y.-C. Kao, S.-J. Jiang, W.-A. Pan, K.-C. Wang, P.-K. Chen, H.-J. Wei, W.-S. Chen, B.-I. Chang, G.-Y. Shi, H.-L. Wu, The epidermal growth factor-like domain of CD93 is a potent angiogenic factor, PLoS ONE 7 (2012), e51647.

[28] H. Guo, S. An, R. Ward, Y. Yang, Y. Liu, X.-X. Guo, Q. Hao, T.-R. Xu, Methods used to study the oligomeric structure of G-protein-coupled receptors, Biosci. Rep. 37 (2017), BSR20160547.

[29] X.-Q. Wei, M. Orchardson, J.A. Gracie, B.P. Leung, B.-M. Gao, H. Guan, W. Niedbala, G.K. Paterson, I.B. McInnes, F.Y. Liew, The sushi domain of soluble IL-15 receptor alpha is essential for binding IL-15 and inhibiting inflammatory and allogenic responses in vitro and in vivo, J. Immunol. Methods 167 (2001) 277–282.

[30] A.S. Llera, F. Viedma, F. Sánchez-Madrid, J. Tormo, Crystal structure of the C-type lectin-like domain from the human hematopoietic cell receptor CD69, J. Biol. Chem. 276 (2001) 7312–7319.

[31] H.-C. Huang, G.-Y. Shi, S.-J. Jiang, C.-S. Shi, C.-M. Wu, H.-Y. Yang, H.-L. Wu, Thrombomodulin-mediated cell adhesion: involvement of its lectin-like domain, J. Biol. Chem. 278 (2003) 46750–46759.

[32] M.K. Ki, M.H. Jeoung, J.R. Choi, S.S. Rho, Y.G. Kwon, H. Shim, J. Chung, H. J. Hong, B.D. Song, S. Lee, Human antibodies targeting the C-type lectin-like domain of the tumor endothelial cell marker clec14a regulate angiogenic properties in vitro, Oncogene 32 (2013) 5449–5457.

[33] N.M. Ayoub, S.K. Jaradat, K.M. Al-Shami, A.E. Alkhalifa, Targeting angiogenesis in breast cancer: current evidence and future perspectives of novel anti-angiogenic approaches, Front. Pharmacol. 13 (2022), 838133.

[34] P. Mammadzada, P.M. Corredoira, H. André, The role of hypoxia-inducible factors in neovascular age-related macular degeneration: a gene therapy perspective, Cell. Mol. Life Sci. 77 (2020) 819–833.

[35] G.M. Tosi, G. Neri, S. Barbera, L. Mundo, B. Parolini, S. Lazzi, R. Lugano, E. Poletto, L. Leoncini, G. Pertile, M. Mongiat, A. Dimberg, F. Galvagni, M. Orlandini, The binding of CD93 to Multimerin-2 promotes choroidal neovascularization, Invest. Ophthalmol. Vis. Sci. 61 (2020) 30.

[36] R. Colladel, R. Pellicani, E. Andreuzzi, A. Paulitti, G. Tarticchio, F. Todaro, A. Colombatti, M. Mongiat, MULTIMERIN2 binds VEGF-A primarily via the carbohydrate chains exerting an angiostatic function and impairing tumor growth, Oncotarget 7 (2016) 2022–2037.

[37] M. Orlandini, S. Nucciotti, F. Galvagni, M. Bardelli, M. Rocchigiani, F. Petraglia, S. Oliviero, Morphogenesis of human endothelial cells is inhibited by DAB2 via Src, FEBS Lett. 582 (2008) 2542–2548.

[38] A.P. Cribbs, A. Kennedy, B. Gregory, F.M. Brennan, Simplified production and concentration of lentiviral vectors to achieve high transduction in primary human T cells, BMC Biotechnol. 13 (2013) 98.

[39] E. Lorenzon, R. Colladel, E. Andreuzzi, S. Marastoni, F. Todaro, M. Schiappacassi, G. Ligresti, A. Colombatti, M. Mongiat, MULTIMERIN2 impairs tumor angiogenesis and growth by interfering with VEGF-A/VEGFR2 pathway, Oncogene 31 (2012) 3136–3147.

[40] F. Galvagni, F. Anselmi, A. Salameh, M. Orlandini, M. Rocchigiani, S. Oliviero, Vascular endothelial growth factor receptor-3 activity is modulated by its association with caveolin-1 on endothelial membrane, Biochemistry 46 (2007) 3998–4005.

[41] D. Stepensky, FRETcalc plugin for calculation of FRET in non-continuous intracellular compartments, Biochem. Biophys. Res. Commun. 359 (2007) 752–758.

[42] C. Boscher, V. Gaonac'h-Lovejoy, C. Delisle, J.-P. Gratton, Polarization and sprouting of endothelial cells by angiopoietin-1 require PAK2 and paxillin-dependent Cdc42 activation, Mol. Biol. Cell 30 (2019) 2227–2239.

[43] M. Mongiat, S. Marastoni, G. Ligresti, E. Lorenzon, M. Schiappacassi, R. Perris, S. Frustaci, A. Colombatti, The extracellular matrix glycoprotein elastin microfibril interface located protein 2: a dual role in the tumor microenvironment, Neoplasia 12 (2010) 294–304.

[44] M. Benvenuti, S. Mangani, Crystallization of soluble proteins in vapor diffusion for x-ray crystallography, Nat. Protoc. 2 (2007) 1633–1651.

[45] W. Kabsch, XDS, Acta Crystallogr. D Biol. Crystallogr. 66 (2010) 125–132.

[46] P.R. Evans, An introduction to data reduction: space-group determination, scaling and intensity statistics, Acta Crystallogr. D Biol. Crystallogr. 67 (2011) 282–292.

[47] M.D. Winn, C.C. Ballard, K.D. Cowtan, E.J. Dodson, P. Emsley, P.R. Evans, R. M. Keegan, E.B. Krissinel, A.G.W. Leslie, A. McCoy, S.J. McNicholas, G. N. Murshudov, N.S. Pannu, E.A. Potterton, H.R. Powell, R.J. Read, A. Vagin, K. S. Wilson, Overview of the CCP4 suite and current developments, Acta Crystallogr. D Biol. Crystallogr. 67 (2011) 235–242.

[48] A. Vagin, A. Teplyakov, Molecular replacement with MOLREP, Acta Crystallogr. D Biol. Crystallogr. 66 (2010) 22–25.

[49] G.N. Murshudov, P. Skubák, A.A. Lebedev, N.S. Pannu, R.A. Steiner, R.A. Nicholls, M.D. Winn, F. Long, A.A. Vagin, REFMAC5 for the refinement of macromolecular crystal structures, Acta Crystallogr. D Biol. Crystallogr. 67 (2011) 355–367.

[50] P. Emsley, B. Lohkamp, W.G. Scott, K. Cowtan, Features and development of Coot, Acta Crystallogr. D Biol. Crystallogr. 66 (2010) 486–501.

[51] R.A. Laskowski, M.W. MacArthur, D.S. Moss, J.M. Thornton, PROCHECK: a program to check the stereochemical quality of protein structures, J. Appl. Crystallogr. 26 (1993) 283–291.

[52] E. Krissinel, K. Henrick, Inference of macromolecular assemblies from crystalline state, J. Mol. Biol. 372 (2007) 774–797.

[53] L. Potterton, S. McNicholas, E. Krissinel, J. Gruber, K. Cowtan, P. Emsley, G. N. Murshudov, S. Cohen, A. Perrakis, M. Noble, Developments in the CCP4 molecular-graphics project, Acta Crystallogr. D Biol. Crystallogr. 60 (2004) 2288–2894.